# Chapter 13
# Lattice-Gas Cellular Automaton Modeling of Emergent Behavior in Interacting Cell Populations

**Haralambos Hatzikirou and Andreas Deutsch**

## 13.1 Introduction

Biological organisms are complex systems characterized by collective behavior emerging out of the interaction of a large number of components (molecules and cells). In complex systems, even if the basic and local interactions are perfectly known, it is possible that the global (collective) behavior obeys new laws that are not obviously extrapolated from the individual properties. Only an understanding of the dynamics of collective effects at the molecular, and cellular scale allows answers to biological key questions such as: what enables ensembles of molecules to organize themselves into cells? How do ensembles of cells create tissues and whole organisms? Key to solving these problems is the design and analysis of appropriate mathematical models for spatio-temporal pattern formation. Early models of spatio-temporal pattern formation focused on the dynamics of diffusible morphogen signals and have been formulated as partial differential equations (e.g. [25]). Today, it is realized that, in addition to diffusible signals, the role of cells in morphogenesis can not be neglected. Living cells possess migration strategies that go far beyond the merely random displacements of non-living molecules (diffusion). More and more evidence has been collected how populations of interacting and migrating cells can in a self-organized manner contribute to the formation of order in a developing organism. It has been realized, that both the particular type of cell interaction and migration are crucial and suitable combinations allow for a wide range of patterns. The question is: What are appropriate mathematical models for analyzing organization principles of moving and interacting discrete cells? It has turned out that cellular automata (CA), in particular lattice-gas cellular automata (LGCA) can model the interplay of cells with themselves and their heterogeneous environment [15]. These models describe interaction at a cell-based (microscopic) scale. Cell-based models (for a review see [18]) are required if one is attempting to extract the organization

H. Hatzikirou (✉)
Center for Information Services and High Performance Computing, Technische Universität Dresden, Nöthnitzerstr. 46, 01069 Dresden, Germany
e-mail: haralambos.hatzikirou@tu-dresden.de

A.G. Hoekstra et al. (eds.), *Simulating Complex Systems by Cellular Automata*, Understanding Complex Systems, DOI 10.1007/978-3-642-12203-3_13,

principles of interacting cell systems down to length scales of the order of a cell diameter in order to link the individual (microscopic) cell dynamics with a particular collective (macroscopic) phenomenon.

Cellular automata (CA) are discrete dynamical systems. They were introduced by J. von Neumann and S. Ulam in the 1950s in an attempt to model biological self-reproduction [31]. Since then, it has become clear that CA have a much broader potential as models for physical, chemical and biological self-organization. In particular, CA models have been proposed for a large number of biological applications for studying the emergence of collective macroscopic behavior emerging from the microscopic interaction of individual components, such as molecules, cells or organisms [15]. However, currently there exists a huge jungle of different rules for often the same or similar processes (e.g. for random walk or proliferation). Therefore, there is need for a specification and classification of CA rules. Such a classification approach has comprehensively been performed for one-dimensional automata [33]. Furthermore, examples of successful analysis of CA models beyond purely visual inspection of simulation outcomes are still rare.

Here, we introduce lattice-gas cellular automata (LGCA) as models for collective behavior emerging from microscopic migration and interaction processes [15, 20]. LGCA represent a class of CA whose structure facilitates mathematical analysis. Implementing movement of individuals in traditional cellular automaton models is not straightforward, as one site in a lattice can typically only contain one individual, and consequently movement of individuals cause collisions when two individuals move to the same empty site. In a lattice-gas model this problem is avoided by having separate channels for each direction of movement and imposing an exclusion principle. Furthermore, the update rule is split into two parts which are called interaction and propagation, respectively. The interaction rule of LGCA can be compared with the update rule for CA in that it assigns new states to each particle based on the states of the sites in a local neighborhood. After the interaction/collision step the state of each node is propagated to a neighboring node. This split of the update rule allows for transport of particles while keeping the rules simple. The emergent collective behavior, e.g. spatio-temporal pattern formation in a LGCA shows up in the macroscopic limit which can be derived from a theory of statistical mechanics on a lattice. In place of discrete particles, Lattice Boltzmann (LB) models deal with continuous distribution functions which interact locally and which propagate after collision to the next neighbor node. LB models can be interpreted as mean-field approximations of LGCA. LGCA and LB models have been originally introduced as models of fluid flow [20]. Meanwhile, LGCA and LB models have found numerous applications in physics, chemistry and more recently biology [13, 15, 17, 28, 32].

In particular, we present two examples for LGCA models. The first example focuses on the collective behavior of moving and proliferating cells which is characterized by the emergence of a traveling wavefront. We derive a macroscopic description and, by means of a cut-off mean-field analysis, we calculate the wavefront speed. This analysis enables us to estimate (macroscopic) cell population spreading based on established microscopic cell properties, such as cell motility and proliferation rate. The second example addresses the precise interplay of moving cells with their typically heterogeneous environment which is crucial for central biological

processes as embryonic morphogenesis, wound healing, immune reactions or tumor growth. We introduce a LGCA model of cell migration in different biological environments. Then we analyze the emergent migration features of the cell population under specific environmental constraints.

## 13.2 Lattice-Gas Cellular Automata

We define a d-dimensional regular lattice $\mathcal{L} = L_1 \times \cdots \times L_d \subset \mathbb{Z}^d$, where $L_1, ..., L_d$ are the numbers of nodes in each lattice dimension. Here, we will refer to two-dimensional models ($d = 2$). Particles move on the discrete lattice with discrete velocities, i.e. they hop at discrete time steps $k \in \mathbb{N}$ from a given node to a neighboring one. A set of velocity channels $(\mathbf{r}, \mathbf{c}_i),\ i = 1, \ldots, b$, is associated with each node $\mathbf{r} \in \mathcal{L} \subset \mathbb{Z}^d$ of the lattice. The parameter $b$ is the *coordination number*, i.e. the number of velocity channels on a node which coincides with the number of nearest neighbors on a given lattice. In particular, the set of velocity channels for the square lattice as considered here, is represented by the two-dimensional channel velocity vectors $\mathbf{c}_1 = \begin{pmatrix} 1 \\ 0 \end{pmatrix}, \mathbf{c}_2 = \begin{pmatrix} 0 \\ 1 \end{pmatrix}, \mathbf{c}_3 = \begin{pmatrix} -1 \\ 0 \end{pmatrix}, \mathbf{c}_4 = \begin{pmatrix} 0 \\ -1 \end{pmatrix}$ (see Fig. 13.1). In addition, there is a variable number $\beta \in \mathbb{N}_0 = \mathbb{N} \cup \{0\}$ of rest channels (zero-velocity channels), $(\mathbf{r}, \mathbf{c}_i),\ b < i \leq b + \beta$. Furthermore, an exclusion principle is imposed. This requires, that not more than one particle can be at the same node within the same channel. As a consequence, each node $\mathbf{r}$ can host up to $\tilde{b} = b + \beta$ particles, which are distributed in different channels $(\mathbf{r}, \mathbf{c}_i)$ with at most one particle per channel. Accordingly, node state $\eta(\mathbf{r})$ is given by

$$\eta(\mathbf{r}) := \big(\eta_1(\mathbf{r}), \ldots, \eta_{\tilde{b}}(\mathbf{r})\big),$$

where $\eta(\mathbf{r})$ is called *node configuration* and the quantities $\eta_i(\mathbf{r}) \in \{0, 1\}, i = 1, \ldots, \tilde{b}$ are called *occupation numbers*, which are Boolean variables that indicate the presence ($\eta_i(\mathbf{r}) = 1$) or absence ($\eta_i(\mathbf{r}) = 0$) of a particle in the respective channel $(\mathbf{r}, \mathbf{c}_i)$. Therefore, the set of elementary states $\mathcal{E}$ of a single node is given by

$$\mathcal{E} = \{0, 1\}^{\tilde{b}}.$$

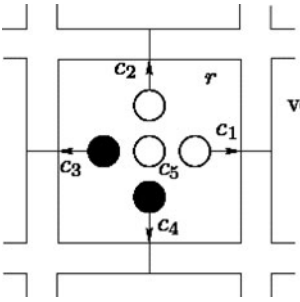


$$\begin{aligned} \tilde{b} &= 5 \\ \text{velocity channels:} &\quad (r, c_1),\ (r, c_2),\ (r, c_3),\ (r, c_4) \\ \text{rest channel:} &\quad (r, c_5) \\ \eta(r) &= \big(\eta_1(r), \eta_2(r), \eta_3(r), \eta_4(r), \eta_5(r)\big) \\ &= \big(0, 0, 1, 1, 0\big) \\ \rho(\mathbf{r}) &= 2 \end{aligned}$$

**Fig. 13.1** Node configuration: channels of node $\mathbf{r}$ in a two-dimensional square lattice ($b = 4$) with one rest channel ($\beta = 1$). *Filled dots* denote the presence of a particle in the respective channel

The *node density* is the total number of particles present at a node $\mathbf{r}$ and time $k \in \mathbb{N}$ denoted by

$$n(\mathbf{r}, k) := \sum_{i=1}^{\tilde{b}} \eta_i(\mathbf{r}, k).$$

For any node $\mathbf{r} \in \mathcal{L}$, the nearest lattice neighborhood $\mathcal{N}_b(\mathbf{r})$ is a finite list of neighboring nodes and is defined as

$$\mathcal{N}_b(\mathbf{r}) := \{\mathbf{r} + \mathbf{c}_i \ : \ \mathbf{c}_i \in \mathcal{N}_b \ , \ i = 1, \ldots, b\} \ .$$

Figure 13.1 gives an example of the representation of a node on a two-dimensional lattice with $b = 4$ and $\beta = 1$, i.e. $\tilde{b} = 5$.

### *13.2.1 Dynamics in Lattice-Gas Cellular Automata*

The dynamics of a LGCA arises from the application of superpositions of local (probabilistic) *interaction* and deterministic *propagation* (transport) steps applied simultaneously to all lattice nodes and at each discrete time step. The definitions of these steps have to satisfy the exclusion principle, i.e. two or more particles are not allowed to occupy the same channel.

According to a model-specific *interaction* rule ($\mathcal{R}^{\mathrm{C}}$), particles can change channels (see Fig. 13.2) and/or are created or destroyed. The temporal evolution of a state $\eta(\mathbf{r}, k) \in \{0, 1\}^{\tilde{b}}$ in a LGCA is determined by the temporal evolution of the occupation numbers $\eta_i(\mathbf{r}, k)$ for each $i \in \{1, \ldots, \tilde{b}\}$ at node $\mathbf{r}$ and time $k$. Accordingly, the pre-interaction state $\eta_i(\mathbf{r}, k)$ is replaced by the post-interaction state $\eta_i^{\mathrm{C}}(\mathbf{r}, k)$ determined by

$$\eta_i^{\mathrm{C}}(\mathbf{r}, k) = \mathcal{R}_i^{\mathrm{C}}\big(\{\eta(\mathbf{r}, k) | \mathbf{r} \in \mathcal{N}_b(\mathbf{r})\}\big), \tag{13.1}$$

$$\eta^{\mathrm{C}}(\mathbf{r}, k) = \mathcal{R}^{\mathrm{C}}\big(\{\eta(\mathbf{r}, k) | \mathbf{r} \in \mathcal{N}_b(\mathbf{r})\}\big) = \Big(\mathcal{R}_i^{\mathrm{C}}\big(\{\eta(\mathbf{r}, k) | \mathbf{r} \in \mathcal{N}_b(\mathbf{r})\}\big)\Big)_{i=1}^{\tilde{b}},$$

realized with probability $\mathbb{P}\big(\eta \ \rightarrow \ \eta^{\mathrm{C}}\big)$ and $\eta^{\mathrm{C}} \in (0, 1)^{\tilde{b}}$, which is the time-independent probability for transition from the pre-interaction to the post-interaction node state.

In the deterministic *propagation* or streaming step (P), all particles are moved simultaneously to nodes in the direction of their velocity, i.e. a particle residing in channel $(\mathbf{r}, \mathbf{c}_i)$ at time $k$ is moved to another channel $(\mathbf{r} + m\mathbf{c}_i, \mathbf{c}_i)$ during one time step (Fig. 13.3). Here, $m \in \mathbb{N}_0$ determines the *single particle speed* and $m\mathbf{c}_i$ the *translocation* of the particle. Because all particles residing at the same velocity channel move the same number $m$ of lattice units, the exclusion principle is maintained. Particles occupying rest channels do not move since they have "zero

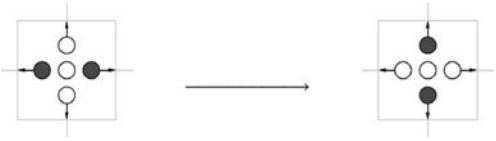

**Fig. 13.2** Example of a possible interaction of particles at a node $\mathbf{r}$; *filled dots* denote the presence of a particle in the respective channel. *Arrows* indicate channel directions

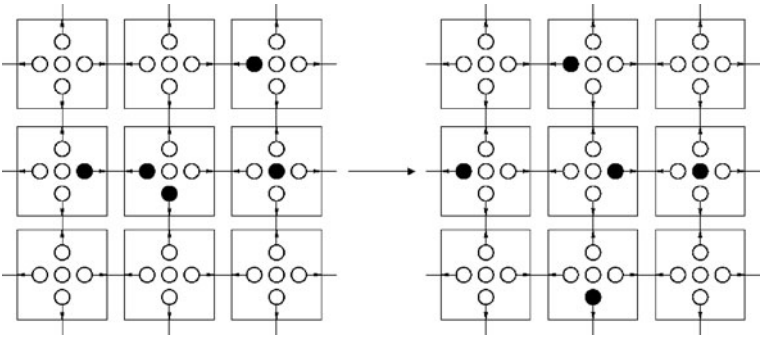

**Fig. 13.3** Propagation in a two-dimensional square lattice with speed $m = 1$; lattice configurations before and after the propagation step; *filled dots* denote the presence of a particle in the respective channel

velocity". In terms of occupation numbers, the state of channel $(\mathbf{r} + m\mathbf{c}_i, \mathbf{c}_i)$ after propagation is given by

$$\eta_i(\mathbf{r} + m\mathbf{c}_i, k + \tau) = \eta_i^{\mathrm{P}}(\mathbf{r}, k), \tag{13.2}$$

where $\tau \in \mathbb{N}$ is the automaton's time-step. We note that the propagation operator is mass and momentum conserving. Hence, if only the propagation step was applied then particles would simply move along straight lines in directions corresponding to particle velocities.

Combining interactive dynamics (C), Eq. (13.1) with propagation (P), Eq. (13.2) implies that

$$\eta_i(\mathbf{r} + m\mathbf{c}_i, k + \tau) = \eta_i^{\mathrm{CP}}(\mathbf{r}, k)\,. \tag{13.3}$$

This can be rewritten as the *microdynamical difference equations*

$$\eta_i(\mathbf{r}+m\mathbf{c}_i, k+\tau) - \eta_i(\mathbf{r}, k) = \eta_i^{\mathrm{CP}}(\mathbf{r}, k) - \eta_i(\mathbf{r}, k) =: C_i(\eta_{\mathcal{N}(\mathbf{r})}(k)),\ i = 1, \ldots, \tilde{b}, \tag{13.4}$$

where we define $C_i$ as the *change in the occupation number* due to interaction. It is given by

$$C_i(\eta_{\mathcal{N}(\mathbf{r})}(k)) = \begin{cases} 1, \text{ creation of a particle in channel } (\mathbf{r}, \mathbf{c}_i) \\ 0, \text{ no change in channel } (\mathbf{r}, \mathbf{c}_i) \\ -1, \text{ annihilation of a particle in channel } (\mathbf{r}, \mathbf{c}_i). \end{cases} \tag{13.5}$$

## 13.3 A LGCA Model for Growing Cell Populations

Growth processes can be found in almost any scientific field, such as physics, ecology, sociology, epidemiology, biology etc. In particular in biology, growth processes play a central role in phenomena related to embryonic development or diseases such as tumor growth. Here, we introduce a microscopic birth/death cell process which results in a traveling front behavior at the macroscopic level.

### *13.3.1 Definition of the LGCA Model*

Automaton dynamics arise from the repetition of three rules (operators): Propagation (P), reorientation (O) and growth (R). In particular, cell motion is defined by the combination of the reorientation and the propagation operators while the growth operator controls the change of the local number of cells at a node.

The reorientation operator is responsible for the redistribution of cells within the velocity channels of a node, providing a new node velocity distribution (see Fig. 13.4). Here, we assume that individual cells perform random walks. The corresponding transition probabilities are

$$\mathbb{P}(\eta \to \eta^{\mathrm{O}})(\mathbf{r}, \cdot) = \frac{1}{Z}\delta\big(n(\mathbf{r}, \cdot), n^{\mathrm{O}}(\mathbf{r}, \cdot)\big), \tag{13.6}$$

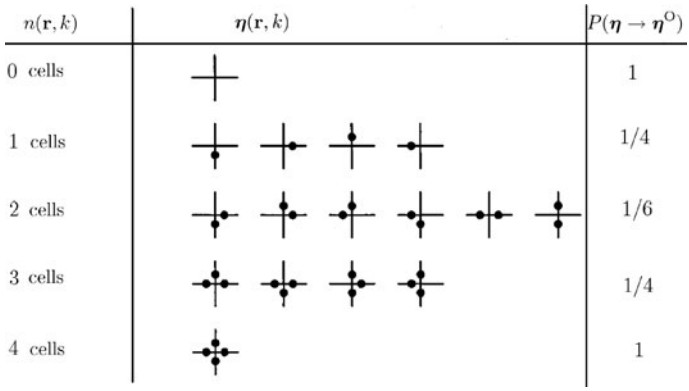


**Fig. 13.4** Reorientation rule of random motion: The *left column* corresponds to the possible node densities $n(\mathbf{r}, \cdot)$, with node capacity $\tilde{b} = 4$. The *central column* provides all possible node configurations, while the *right column* indicates the respective transition probabilities (Eq. (13.6))

where the normalization factor $Z = \sum_{\eta^{\mathrm{O}}(r,\cdot)} \delta\big(n(\mathbf{r},\cdot), n^{\mathrm{O}}(\mathbf{r},\cdot)\big)$ corresponds to the equivalence class defined by the value of the pre-interaction node density $n(\mathbf{r},\cdot)$.

#### 13.3.1.1 Growth (R)

We define a stochastic birth/death process for the cells as follows:

- **Birth**: We assume that the proliferation rule depends on the node capacity $\tilde{b}$, which is interpreted as a microscopic volume exclusion. For the creation of a new cell on a node, the existence of at least one cell and at least one free channel are required, i.e.:

$$\mathcal{R}_i(\mathbf{r},\cdot) = \xi_i(\mathbf{r},\cdot)(1-\eta_i(\mathbf{r},\cdot)), \tag{13.7}$$

  where $\xi_i(\mathbf{r},\cdot)$'s are random Boolean variables, with $\sum_{i=1}^{\tilde{b}} \xi_i(\mathbf{r},\cdot) = 1$, and the corresponding probabilities are:

$$\mathbb{P}(\xi_i(\mathbf{r},\cdot)=1) = r_M \frac{\sum_{i=1}^{\tilde{b}} \eta_i(\mathbf{r},\cdot)}{\tilde{b}}. \tag{13.8}$$

  Here, $r_M$ is the probability of occupying a channel, if at least one cell exists on the node. The growth law, as defined above, is also known as *carrying capacity-limited* or *contact-inhibited* growth.
- **Death**: We assume that a certain nutrient availability implies a maximum node occupancy $C$, i.e. the node nutrient supply cannot support more than $C \leq \tilde{b}$ living cells. Thus, we define a death rate for each cell that ensures the existence of at most $C$ cells per node:

$$r_d = \frac{\tilde{b}-C}{\tilde{b}} r_M, \tag{13.9}$$

  where the factor $\frac{\tilde{b}-C}{\tilde{b}}$ is a dimensionless quantity.

### *13.3.2 Microdynamical Equations*

The above defined dynamics is fully specified by the following microdynamical equations:

$$\eta_i^{\mathrm{R}}(\mathbf{r},k) = \eta_i(\mathbf{r},k) + \mathcal{R}_i(\mathbf{r},k), \tag{13.10}$$

$$\eta_i(\mathbf{r}+m\mathbf{c}_i, k+\tau) = \sum_{j=1}^{\tilde{b}} \mu_j(\mathbf{r},k)\eta_j^{\mathrm{R}}(\mathbf{r},k). \tag{13.11}$$

Equation (13.10) refers to the application of the *growth* operator (R), which assigns a new occupation number for a given channel through a stochastic growth process. The second equation (13.11) refers to the *redistribution* of cells on the velocity

channels and the *propagation* to the neighboring nodes, corresponding to the random walk as introduced in the previous chapter.

The $\mu_j(\mathbf{r}, k) \in \{0, 1\}$ are Boolean random variables which select only one of the $\tilde{b}$ terms of the rhs of Eq. (13.11). Therefore, they should satisfy the relation $\sum_{j=1}^{\tilde{b}} \mu_j(\mathbf{r}, k) = 1$. As stated above, we implement the random walk as a simple reshuffling of the cells within the node channels that leads to the probability of choosing a channel: $\langle \mu_j \rangle = 1/\tilde{b}$, for $j = 1, ..., \tilde{b}$. The terms $\mathcal{R}_i(\mathbf{r}, k) \in \{0, 1\}$, for $i = 0, \ldots \tilde{b}$ (Eq. (13.7)) represent birth/death processes, i.e. creation/annihilation of cells in channel $i$ defined by the growth rule, which are applied to each channel independently.

### *13.3.3 Simulations*

We have simulated our LGCA model on a two-dimensional $100 \times 100$ lattice for 150 time steps. In Fig. 13.5, we show simulations for different times, for fixed maximum

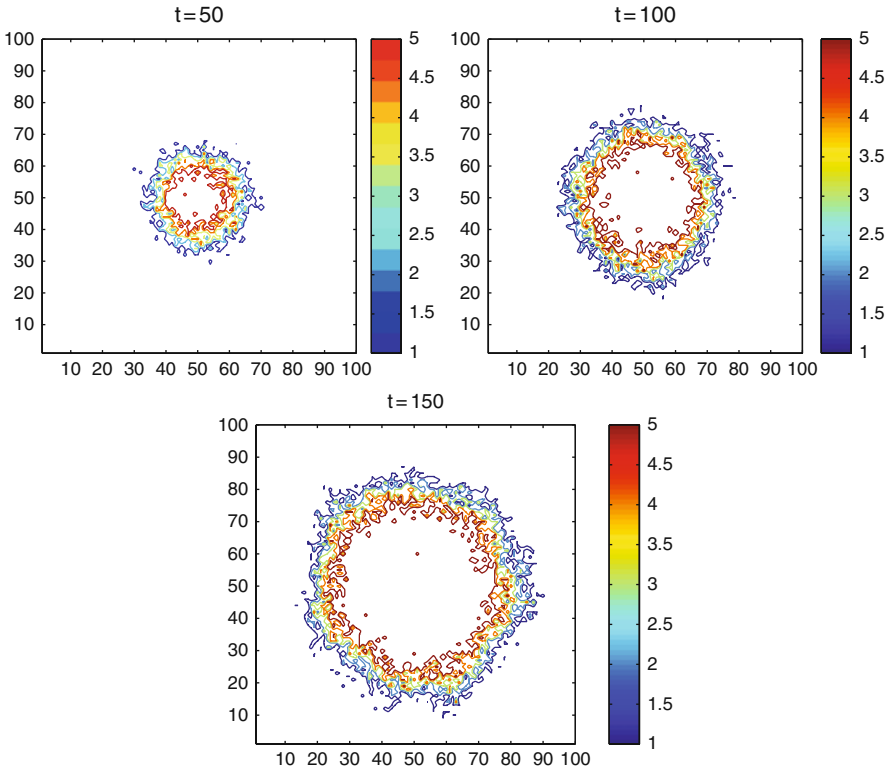


**Fig. 13.5** Typical simulations of the spatio-temporal evolution of the LGCA growth process starting from an initial fully occupied cluster of nodes in the center of the lattice. The three figures show snapshots of the same simulation at different times. The different grey levels encode the node density

occupancy $C = \tilde{b}$ and for fixed proliferation rate $r_M = 0.01$. The initial condition is just a small disc. From the simulations, we conclude the following:

(01) The pattern evolving in simulations from a localized initial occupation is an isotropically growing disc.
(02) Furthermore, simulations indicate a moving front along which the occupancy of the initially empty nodes is increasing from zero particles to the maximum occupancy $C$.

In order to get further insight into the macroscopic behavior of the growth process, we use a different simulation setup. We consider a "tube", especially a $2000 \times 10$ lattice with periodic boundary condition on the $L_2$-axis, and a thin stripe of cells as initial condition (Fig. 13.6). A typical simulation time lasts for 2000 time steps. The result of our simulations is a propagating 2D traveling front along the $L_1$-axis, mimicking a "growing tube". This setting has the following advantages:

- One can project the system to one dimension by averaging the concentration profile along the $L_2$-axis, i.e. $n(r_x, k) = \frac{1}{|L_2|} \sum_{r_y \in |L_2|} n(\mathbf{r}, k)$.
- The front is well-defined as the mean position of the foremost cells.

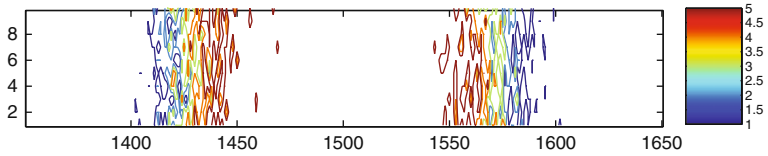


**Fig. 13.6** Typical simulation on a "tubular" lattice, i.e. with periodic boundary condition along the y-axis. The different grey levels denote the node density. In the central region of the figure, the *white part* denotes nodes with maximum density

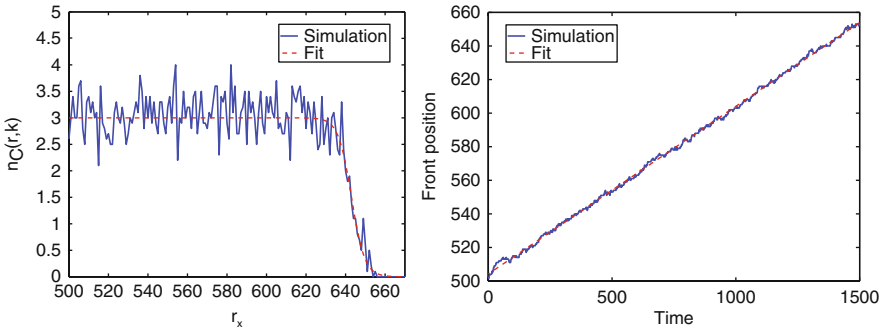


**Fig. 13.7** *Left*: Snapshot of the average concentration profile along the $L_1$-axis, i.e. $n_x(k) = n(r_x, k) = \frac{1}{|L_2|} \sum_{r_y \in |L_2|} n(\mathbf{r}, k)$. Here, the maximum occupancy is considered as $C = 3$. *Right*: Linear growth of the front distance from its initial position, denoted as front position. The slope of the line defines the speed of the invasion

- The diffusive dynamics of the front relaxes faster than the discoidal 2D evolution.
- The front profile relaxes to an almost steady state shape, which moves almost uniformly along the $L_1$-axis.

The goal is to predict the front velocity. In the following section, we provide the details of the front analysis. Finally, we observe that the front evolves linearly in time, as shown in Fig. 13.7 (right).

## 13.4 Analysis

In this section, we analyze the behavior of our growth LGCA model. By means of a mean-field approximation, we derive a partial differential equation that describes the automaton's macroscopic behavior. Subsequently, we introduce a cut-off in the mean-field description and we calculate the speed of the invasive front.

### *13.4.1 Mean-Field Approximation*

As seen above, our LGCA is governed by the microdynamical equations (13.10) and (13.11). By averaging Eqs. (13.10) and (13.11) and by using the mean-field approximation, we can obtain the lattice Boltzmann equation (LBE)

$$f_i(\mathbf{r}+m\mathbf{c}_i, k+\tau) - f_i(\mathbf{r}, k) = \sum_{j=1}^{\tilde{b}} \Omega_{ij} f_j(\mathbf{r}, k) + \sum_{j=1}^{\tilde{b}} (\delta_{ij} + \Omega_{ij}) \tilde{\mathcal{R}}_j(\mathbf{r}, k), \quad (13.12)$$

where the matrix $\Omega_{ij} = 1/\tilde{b} - \delta_{ij}$ is the transition matrix of the underlying shuffling process. Moreover, we assume that the mean-field reaction term is independent of the particle direction, i.e. $\tilde{\mathcal{R}}_i = F(\rho)/\tilde{b}$, where $F(\rho)$ is the mean-field cell reaction term for a single node. Using the mean-field approximation, we obtain the reaction term $\tilde{\mathcal{R}}_i$:

$$\tilde{\mathcal{R}}_i(\mathbf{r}, k) = r_M f_i(\mathbf{r}, k)\Big(1 - \frac{r_D}{r_M} - f_i(\mathbf{r}, k)\Big). \quad (13.13)$$

### *13.4.2 Macroscopic Dynamics*

In order to derive a macroscopic description, we use the Chapman-Enskog methodology. Here, we assume diffusive scaling as

$$\mathbf{x} = \varepsilon \mathbf{r} \text{ and } t = \varepsilon^2 k, \quad (13.14)$$

where $(\mathbf{x}, t)$ are the continuous variables as $\varepsilon \to 0$. Using the spatio-temporal scaling relation Eq. (13.14) and replacing the first part of Eq. (13.12) by its Taylor expansion leads to:

$$f_i(\mathbf{r} + m\mathbf{c}_i, k + \tau) - f_i(\mathbf{r}, k) = \Big(\varepsilon^2 \tau \partial_t + \varepsilon^4 \frac{\tau^2}{2} \partial_{tt} + \varepsilon m(\mathbf{c}_i \cdot \nabla) + \varepsilon^2 \frac{m^2}{2} (\mathbf{c}_i \cdot \nabla)^2 + \varepsilon^3 \tau m \partial_t (\mathbf{c}_i \cdot \nabla)\Big) f_i(\mathbf{r}, k). \tag{13.15}$$

Furthermore, we assume an asymptotic expansion of $f_i$:

$$f_i = f_i^{(0)} + \varepsilon f_i^{(1)} + \varepsilon^2 f_i^{(2)} + \mathcal{O}(\varepsilon^3). \tag{13.16}$$

An important aspect is the scaling of the growth term. We argue that the birth of cells is taking place at a much slower time scale than the motion. The idea is that growth can be considered as a perturbation of cell motion. That means that the dominant process is random cell motion (as it is shown below). The growth rate is assumed to be scaled according to the macroscopic time scaling, i.e.

$$\bar{\mathcal{R}}_i \to \varepsilon^2 \tilde{\mathcal{R}}_i. \tag{13.17}$$

Equation (13.17) implies that the macroscopic rate should be scaled as $r_M = \varepsilon^2 \tilde{r}_M \ll 1$, where $\tilde{r}_M = \mathcal{O}(1)$. Therefore, our approximation is valid only for very low growth rates.

Collecting the equal $\mathcal{O}(\varepsilon)$ terms, we can formally derive a spatio-temporal mean-field macroscopic approximation (for detail see [13]):

$$\partial_t \rho = \frac{m^2}{\tilde{b}\tau} \nabla^2 \rho + \frac{1}{\tau} F(\rho), \tag{13.18}$$

where the term $F(\rho(\mathbf{r}, k)) = \sum_i^{\tilde{b}} \tilde{\mathcal{R}}_i(\mathbf{r}, k)$ is the macroscopic reaction law and using the definitions (13.7) and (13.9) we obtain:

$$F(\rho) = r_M \rho (C - \rho), \tag{13.19}$$

Accordingly, Eq. (13.19) is a kind of *Fisher-Kolmogorov* equation.

#### 13.4.2.1 Cut-off Mean-Field Approximation

The spatio-temporal mean-field approximation (13.18) agrees qualitatively with the system's linearized macroscopic dynamics. However, it fails to provide satisfactory quantitative predictions because it neglects the correlations arising from the local fluctuating dynamics. Studies on chemical fronts have shown that these fluctuations may significantly affect the propagation velocity of the wave front [7, 30].

In order to improve the mean-field approximation (here we characterize it as "naive"), we introduce the *cut-off mean-field approach* [9, 14]. The idea is that the mean-field continuous equation (13.18) fails to describe the behavior of individual cells due to their strong fluctuations at the tip of the front [7]. Therefore, we introduce the cut-off continuous approach which describes the system up to a threshold density $\delta$ of the order of magnitude of one cell, i.e. $\delta \sim \mathcal{O}(1/\tilde{b})$. Let's assume that the full non-linear reactive dynamics can be described by a term $F(\rho)$. Then, the fully non-linear cut-off MF equation reads

$$\partial_t \rho = D\nabla^2 \rho + F(\rho)\Theta(\rho - \delta), \tag{13.20}$$

where $\Theta(\cdot)$ is a Heaviside function. Obviously, if we set $\delta = 0$ then the cut-off PDE will coincide with the naive mean-field approximation.

The cut-off macroscopic description (13.20) adds an extra fixed point, i.e. $\rho(x_i) = \{0, \delta, C\}$, $i = 0, \delta, C$ which breaks the front into three well-defined regions (see Fig. 13.8).

In order to characterize the linearized growth dynamics at the front, we modify the LBE for the cells:

$$\begin{aligned} f_i(\mathbf{r} + \mathbf{c}_i, k+1) - f_i(\mathbf{r}, k) = &\sum_{j=1}^{\tilde{b}} \left( \frac{1}{\tilde{b}} - \delta_{ij} \right) f_j(\mathbf{r}, k) \\ &+ \frac{1}{\tilde{b}} \sum_{j=1}^{\tilde{b}} \left[ \langle \eta_j^{\mathrm{R}}(\mathbf{r}, k) \rangle - f_j(\mathbf{r}, k) \right] \Theta(\rho - \delta), \end{aligned} \tag{13.21}$$

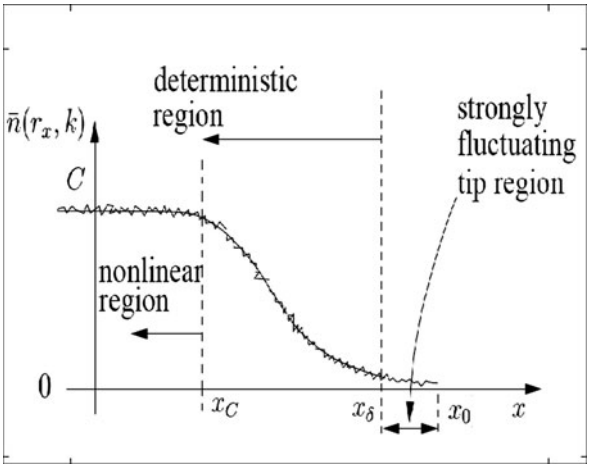


**Fig. 13.8** A sketch of the wavefront as shown in Fig. 13.7 (*left*). We distinguish three regions: (i) $x \in [x_\delta, x_0]$, where $0 < \rho(x) < \delta$: this region represents a highly fluctuating zone, where the cells perform a random walk with almost no proliferation, (ii) $x \in [x_C, x_\delta]$, where $\delta < \rho(x) < C$: this region is a result of non-linear proliferation and cell diffusion and (iii) $x \in [0, x_C]$, where $\rho(x) \simeq C$: this regime represents the bulk of the front (saturated lattice) where no significant changes are observed

where the first summation of the rhs accounts for the reorientation dynamics and the second term is the reactive term of the LBE. Intuitively, the $\Theta$ function "cuts off" the reaction term for local densities lower than the threshold $\delta$. Therefore, for $\rho < \delta$ the cells are influenced only by the random walk dynamics. Moreover from Eq. (13.21), we can easily deduce the nonlinear reaction term of Eq. (13.20):

$$F(\rho) = \sum_{j=1}^{\tilde{b}} \left[ \langle \eta_j^{\mathrm{R}}(\mathbf{r}, k) \rangle - f_j(\mathbf{r}, k) \right]. \tag{13.22}$$

### *13.4.3 Traveling Front Analysis*

In this subsection our goal is to analyze and characterize analytically the observed traveling front behavior. We assume that our system evolves in a "tube", as in Fig. 13.6. Moreover, we make the following assumptions:

(A1) the isotropic evolution of the system allows for the dimension reduction of the analysis to one dimension,
(A2) the system evolves for asymptotically long times, and
(A3) the initial front is sufficiently steep.

Under the assumptions (A1)–(A3), we can conclude that the front relaxes to a time invariant profile. Thus, assuming the translational invariance of the system along the front propagation axis $L_1$, we investigate the steady-state front solutions. The main observable is the average density profile along the axis $L_1$, i.e.

$$\rho(x, t) = \frac{1}{|L_2|} \int_0^{|L_2|} \rho(x, y, t)\, dy \ \in [0, \tilde{b}]. \tag{13.23}$$

Plugging the traveling front solution, $\rho(x, t) = U(x - vt)$, where $x \in L_1$ and $v$ the front velocity into Eq. (13.18), we obtain:

$$DU'' + vU' + \frac{d\tilde{F}}{dU}\Big|_{U=0} = 0, \lim_{\xi \to -\infty} u = U^{\max}, \lim_{\xi \to +\infty} U = 0, U' < 0, \tag{13.24}$$

in terms of the comoving coordinate $\xi = x - vt$ and the prime denotes the derivative with respect to the variable $\xi$. The term $\tilde{F}$ represents the reaction terms in the naive MF approximation expressed in terms of $U$. The front speed for the naive MF can be calculated following the classical methodology [5, 26], i.e.

$$v_{\mathrm{n}} = 2\sqrt{Dr_m}. \tag{13.25}$$

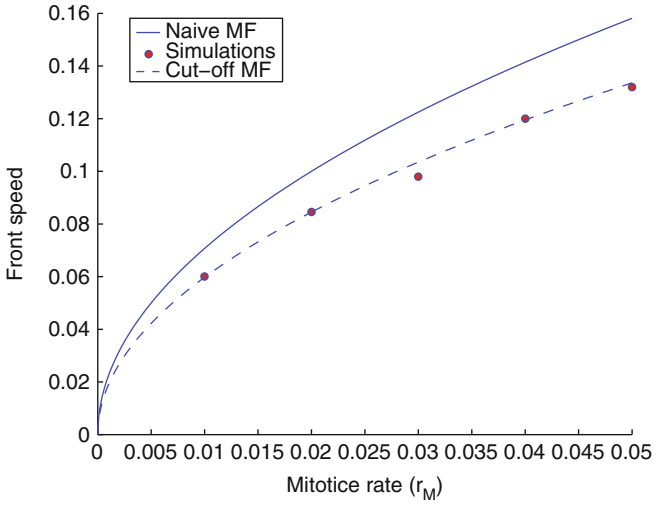


**Fig. 13.9** Comparison of the calculated front speed for the naive and the cut-off MF, i.e. $v_n$ and $v_c$ respectively, against simulations. We observe that the cut-off MF predicts closely the front speed calculated from the simulations for $K \simeq 0.85$

The above speed estimation overestimates the actual front speed found in the simulations. In particular, it is the maximum asymptotic value that the discrete front speed can acquire [9] (see also Fig. 13.9).

The calculation of the front speed under the cut-off MF approximation is more challenging. Following the results proposed by Brunet et al. [9], we can obtain an estimate for the cut-off front speed

$$v_c = 2\sqrt{Dr_M}\left(1 - \frac{K}{\ln^2(\delta)}\right). \tag{13.26}$$

The cut-off front speed estimation includes a correction factor $1 - \frac{K}{\ln^2(\delta)}$, which allows for a better approximation of the actual front speed calculated from the LGCA simulations. The above equation provides a satisfactory description of the system up to the resolution of $\delta$, i.e. to the order of one cell. A reasonable choice of the cut-off would be $\delta = 1/\tilde{b}$. The parameter $K$ is fitted to match quantitatively the simulation results. Several studies have attempted to find an analytical estimate of $K$ but till now this remains an open problem [10]. The cut-off mean-field approximation is a heuristic-phenomenological approach which mimics the leading-order effect of finite population number fluctuations by introducing a cut-off in the MF equation. In Fig. 13.9, we show a comparison of the front speed for varying proliferation rates $r_M$ calculated by the naive MF and the cut-off MF against the front speed obtained from simulations. We observe that for an appropriate choice of $K$ the cut-off MF predicts quantitatively the simulated front speed for all parameter values.

## 13.5 Modelling the Influence of the Microenvironment on Cell Migration

Active migration of tissue cells is essential for a number of biological processes such as inflammation, wound healing, embryogenesis and tumor cell metastasis [6]. Both in natural tissues and artificial environments, such as in vitro tissue cultures, cells can exhibit migratory behavior. In particular, the cellular microenvironment provides the substrate for cell migration. In the following, we provide more details about different cell migration strategies in various environments. Environmental heterogeneity contributes to the complexity of the resulting cellular behaviors. In particular, the cellular microenvironment can either enhance collective motion of cells or direct cell dispersion. Subsequently, we show how a suitable microscopical mathematical model (a LGCA) can contribute to understand the interplay of moving cells with their heterogeneous environment.

### *13.5.1 Cell Migration Strategies*

The cellular microenvironment is a highly heterogeneous medium including the extracellular matrix (ECM) composed of fibrillar structures, collagen matrices, diffusible chemical signals as well as other mobile and immobile cells. Cells move within their environment by responding to their surrounding's stimuli. In addition, cells change their environment locally by producing or absorbing chemicals and/or by degrading the neighboring tissue. This feedback establishes a dynamic relationship between individual cells and the surrounding substrate.

One can distinguish two distinct strategies of cells responding to environmental stimuli: either the cells are following a certain direction and/or the environment imposes only an orientational preference. For example the graded spatial distribution of adhesion ligands along the ECM is thought to influence the direction of cell migration [24], a phenomenon known as haptotaxis [12]. Chemotaxis mediated by diffusible chemotactic signals provides a further example of directed cell motion in a dynamically changing environment. On the other hand, amoeboid and mesenchymal strategies imply an alignment of cells to fibrillar structures. Mesenchymal cells use additionally proteolysis to facilitate their movement and remodel the neighboring tissue (dynamic environment). Table 13.1 summarizes the different cell migration strategies.

**Table 13.1** In this table, we relate the environmental effects to different cell migration strategies. One can distinguish static and dynamic environments. In addition, we identify environments that impart directional or only orientational information for migrating cells (see text for explanations)

| | Static | Dynamic |
|---|---|---|
| Direction | Haptotaxis | Chemotaxis |
| Orientation | Amoeboid | Mesenchymal |

### 13.5.2 LGCA Models of Cell Motion in a Static Environment

In this subsection, we define two LGCA models that describe cell motion in different environments. The mathematical entity that allows for the modeling of such environments is a *tensor field*, which is a collection of different tensors distributed over a spatial domain (for details see [22]). To model cell motion in a given tensor field (environment), we use a special kind of interaction rule for the LGCA dynamics, firstly introduced by Alexander et al. [1]. We consider biological cells as random walkers that are reoriented by maximizing a potential-like term. Assuming that the cell motion is affected by cell–cell and cell–environment interactions, we can define the potential as the sum of these two interactions.:

$$G(\mathbf{r},\cdot)=\sum_j G_j(\mathbf{r},\cdot)=G_{cc}(\mathbf{r},\cdot)+G_{ce}(\mathbf{r},\cdot), \tag{13.27}$$

where $G_j(\mathbf{r},\cdot)$, $j=cc,ce$ is the sub-potential that is related to cell–cell and cell–environment interactions, respectively.

Interaction rules are formulated in such a way that cells preferably reorient into directions which maximize (or minimize) the potential, that is according to the gradients of the potential $\mathbf{G}'(\mathbf{r},\cdot)=\nabla G(\mathbf{r},\cdot)$.

Consider a lattice-gas cellular automaton defined on a two-dimensional lattice with $b$ velocity channels ($b=4$ or $b=6$). Let the *flux* be denoted by

$$\mathbf{J}(\eta(\mathbf{r},\cdot))=\sum_{i=1}^{b}\mathbf{c}_i\eta_i(\mathbf{r},\cdot).$$

The probability that $\eta^C$ is the outcome of an interaction at node $\mathbf{r}$ is defined by

$$\mathbb{P}(\eta\to\eta^{\mathrm{C}}|G(\mathbf{r},\cdot))=\frac{1}{Z}\exp\Big[\alpha F\big(\mathbf{G}'(\mathbf{r},\cdot),\mathbf{J}(\eta^{\mathrm{C}}(\mathbf{r},\cdot))\big)\Big]\delta\big(n(\mathbf{r},\cdot),n^{\mathrm{C}}(\mathbf{r},\cdot)\big), \tag{13.28}$$

where $\eta$ is the pre-interaction state at $\mathbf{r}$ and the Kronecker's $\delta$ assumes the mass conservation of this operator. The sensitivity is tuned by the positive, real parameter $\alpha$. The normalization factor is given by

$$Z=Z(\eta(\mathbf{r},\cdot))=\sum_{\eta^{\mathrm{C}}\in\mathcal{E}}\exp\Big[\alpha F\big(\mathbf{G}'(\mathbf{r},\cdot),\mathbf{J}(\eta^{\mathrm{C}})\big)\Big]\delta\big(n(\mathbf{r},\cdot),n^{\mathrm{C}}(\mathbf{r},\cdot)\big).$$

$F(\cdot)$ is a functional that defines the effect of the $\mathbf{G}'$ gradients on the new configuration. A common choice of $F(\cdot)$ is the inner product $<\cdot,\cdot>$, which favors (or penalizes) the configurations that tend to have the same (or inverse) direction of the gradient $\mathbf{G}'$. Accordingly, the dynamics is fully specified by the following microdynamical equation (for more details see the previous section)

$$\eta_i(\mathbf{r}+\mathbf{c}_i, k+1) = \eta_i^{\mathrm{C}}(\mathbf{r}, k).$$

In the following, we present two stochastic potential-based interaction rules that correspond to the motion of cells in a vector field (i.e. rank 1 tensor field) and a rank 2 tensor field, respectively. We exclude any other cell-cell interactions and we consider that the population consists of a fixed number of cells (mass break conservation).

### 13.5.3 Model I

This model describes cell motion in a static environment that carries directional information expressed by a vector field $\mathbf{E}$. Biologically relevant examples are the motion of cells that respond to fixed integrin[1] concentrations along the ECM (haptotaxis). The spatial concentration differences of integrin proteins constitute a gradient field that creates a kind of "drift" $\mathbf{E}$ [16]. We choose a two dimensional LGCA without rest channels and the stochastic interaction rule of the automaton follows the definition of the potential-based rules (Eq. (13.27) with $\alpha = 1$):

$$\mathbb{P}(\eta \to \eta^{\mathrm{C}})(\mathbf{r}, \cdot) = \frac{1}{Z} \exp\left(\langle \mathbf{E}(\mathbf{r}), \mathbf{J}(\eta^{\mathrm{C}}(\mathbf{r}, \cdot))\rangle\right) \delta\left(n(\mathbf{r}, \cdot), n^{\mathrm{C}}(\mathbf{r}, \cdot)\right), \tag{13.29}$$

where the vector field $\mathbf{G}'(\mathbf{r}) = \mathbf{E}(\mathbf{r})$ is independent of time, and the functional $F$ is defined as:

$$F\left(\mathbf{G}'(\mathbf{r}), \mathbf{J}(\eta^{\mathrm{C}}(\mathbf{r}, \cdot))\right) = \langle \mathbf{E}(\mathbf{r}), \mathbf{J}(\eta^{\mathrm{C}}(\mathbf{r}, \cdot))\rangle. \tag{13.30}$$

We simulate our LGCA for spatially homogeneous $\mathbf{E}$ for various intensities and directions. In Fig. 13.10, we observe the time evolution of a cell cluster under the influence of a given field. We see that the cells collectively move towards the gradient direction and they roughly keep the shape of the initial cluster. The simulations in Fig. 13.11 show the evolution of the system for different fields. It is evident that the "cells" follow the direction of the field and their speed responds positively to an increase of the field intensity.

### 13.5.4 Model II

We now focus on cell migration in environments that promote alignment (orientational changes). Examples of such motion are provided by neutrophil or leukocyte movement through the pores of the ECM, the motion of cells along fibrillar tissues

[1] Integrins are receptors that mediate attachment between a cell and the tissues surrounding it, which may be other cells or the extracellular matrix (ECM).

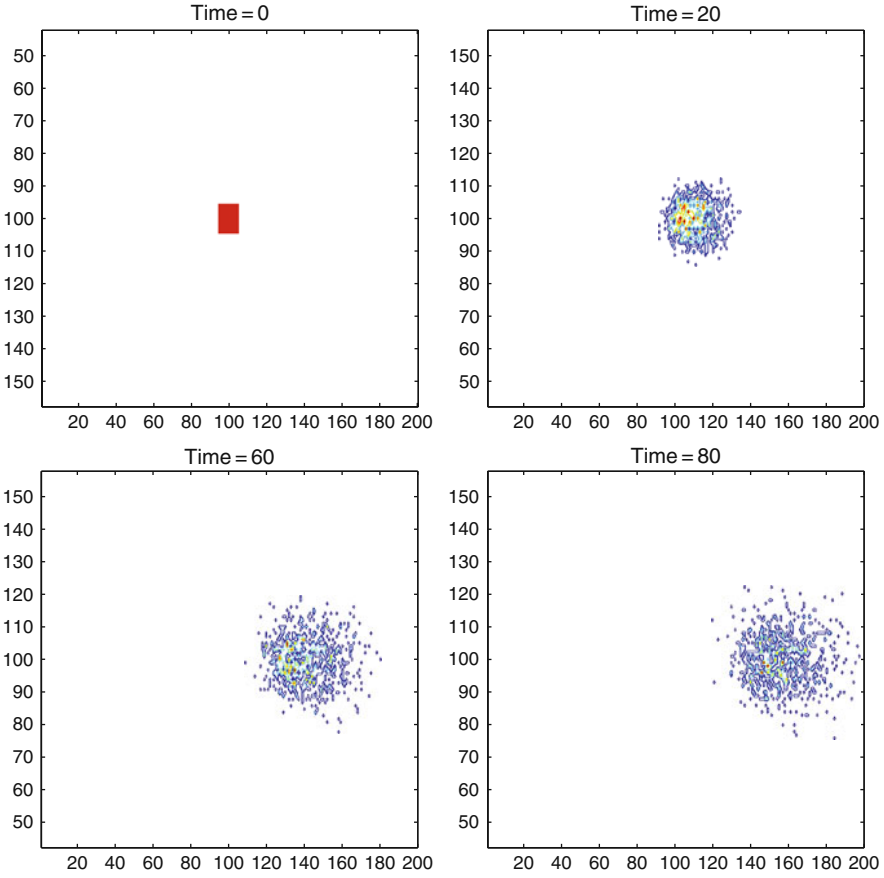


**Fig. 13.10** Time evolution of a cell population under the effect of a field $\mathbf{E} = (1,0)$. One can observe that the environmental drive moves all the cells of the cluster into the direction of the vector field. Different grey levels represent different cell densities

or the motion of glioma cells along fiber tracts. Such an environment can be modeled by a second rank tensor field representing a spatial anisotropy along the tissue. In each point, a tensor (i.e. a matrix) informs the cells about the local orientation and strength of the anisotropy and proposes a principle (local) axis of movement. For instance, the brain's fibre tracts impose a spatial anisotropy and their strength of alignment affects the strength of anisotropy.

Here, we use the information of the principal eigenvector of the tensor (that encodes the environmental influence) which defines the local principle axis of cell movement. Thus, we end up again with a vector field but in this case we exploit only the orientational information of the vector. The new rule for cell movement in an "oriented environment" is:

$$\mathbb{P}(\eta \to \eta^{\mathrm{C}})(\mathbf{r},\cdot) = \frac{1}{Z}\exp\left(\left|\langle \mathbf{E}(\mathbf{r}), \mathbf{J}(\eta^{\mathrm{C}}(\mathbf{r},\cdot))\rangle\right|\right)\delta\left(n(\mathbf{r},\cdot), n^{\mathrm{C}}(\mathbf{r},\cdot)\right). \qquad (13.31)$$

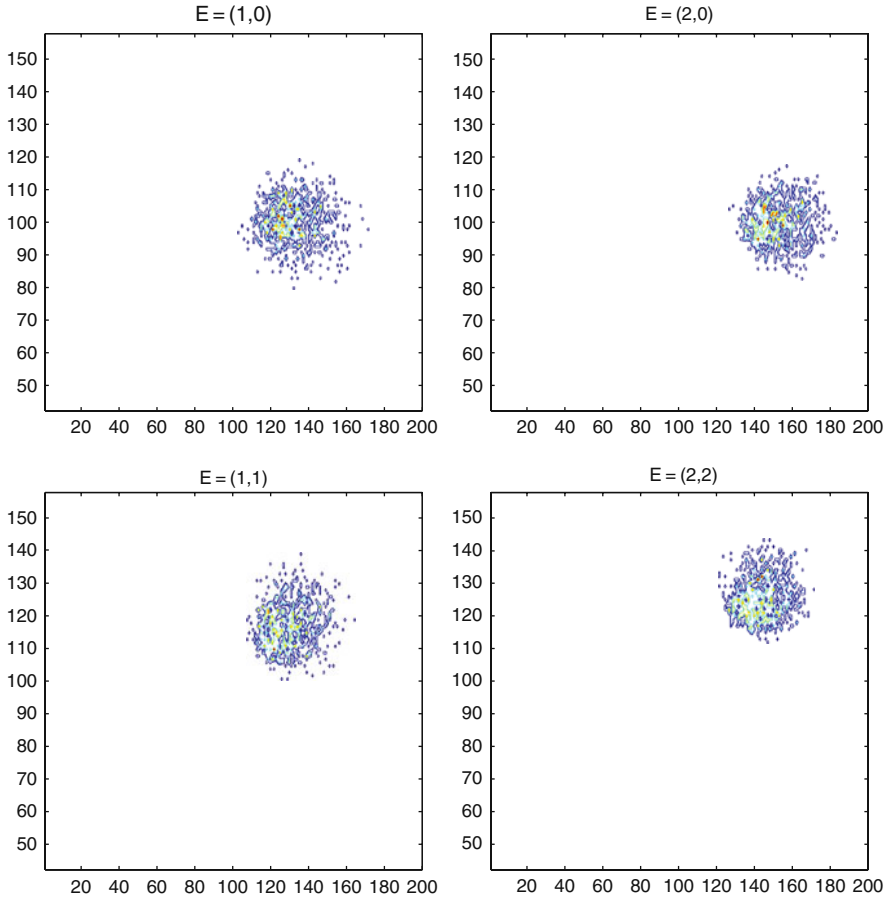


**Fig. 13.11** Time evolution of the cell population under the influence of different fields (after 100 time steps). Increasing the strength of the field, we observe that the cell cluster is moving faster in the direction of the field. This behavior is characteristic of a haptotactically moving cell population. The initial condition is a small cluster of cells in the center of the lattice. Different grey levels indicate different cell densities (as in Fig. 13.10)

where the vector field $\mathbf{G}'(\mathbf{r}) = \mathbf{E}(\mathbf{r})$, is independent of time, and the functional $F$ is defined as:

$$F\big(\mathbf{G}'(\mathbf{r}), \mathbf{J}(\eta^{\mathrm{C}}(\mathbf{r}, \cdot))\big) = \big|\langle \mathbf{E}(\mathbf{r}), \mathbf{J}(\eta^{\mathrm{C}}(\mathbf{r}, \cdot))\rangle\big|. \tag{13.32}$$

In Fig. 13.12, we show the time evolution of a simulation of model II for a given field. Figure 13.13 displays the typical resulting patterns for different choices of tensor fields. We observe that the anisotropy leads to the creation of an ellipsoidal

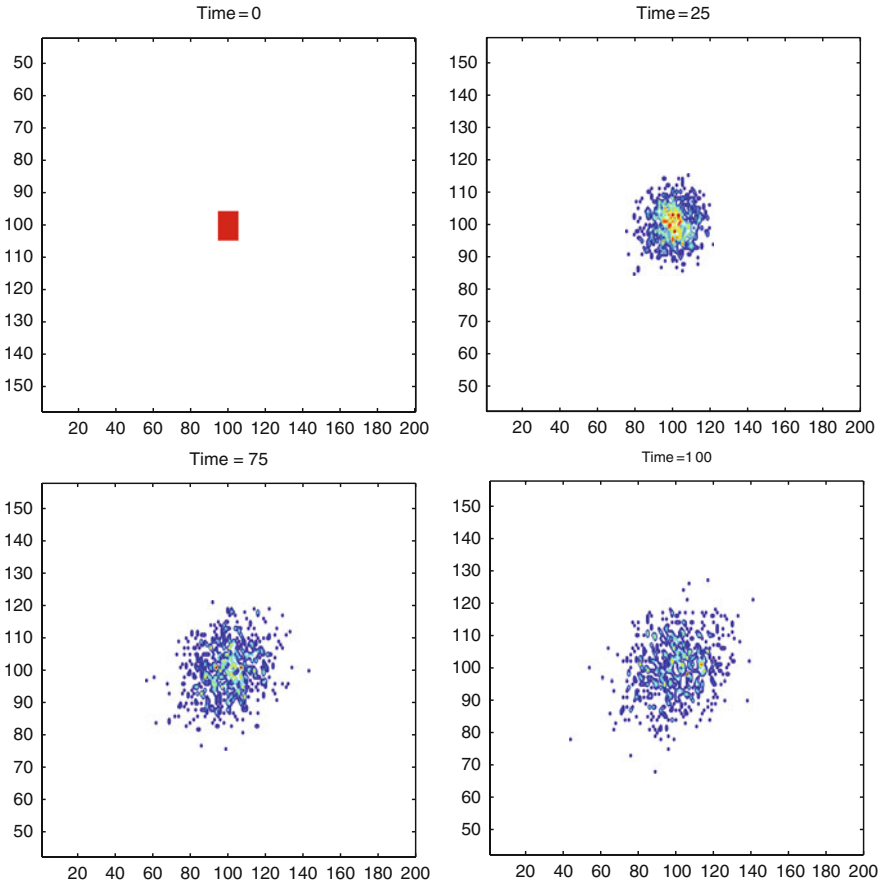


**Fig. 13.12** Time evolution of a cell population under the effect of a tensor field with principal eigenvector (principal orientation axis) $\mathbf{E} = (2,2)$. We observe cell alignment along the orientation of the axis defined by E, as time evolves. Moreover, the initial rectangular shape of the cell cluster is transformed into an ellipsoidal pattern with principal axis along the field **E**. Different grey levels indicate different cell densities (as in Fig. 13.10)

pattern, where the length of the main ellipsoid's axis correlates positively with the anisotropy strength.

This rule can be used to model the migration of glioma cells within the brain. Glioma cells tend to spread faster along fiber tracts. Diffusion Tensor Imaging (DTI) is a Magnetic Resonance Imaging (MRI) based method that provides the local anisotropy information in terms of diffusion tensors. High anisotropy points belong to the brain's white matter, which consists of fiber tracks. A preprocessing of the diffusion tensor field allows the extraction of the principle eigenvectors of the diffusion tensors, that provides us with the local principle axis of motion. By considering a proliferative cell population, as in [21], and using the resulting eigenvector field we can model and simulate glioma cell invasion. In Fig. 13.14, we simulate an example

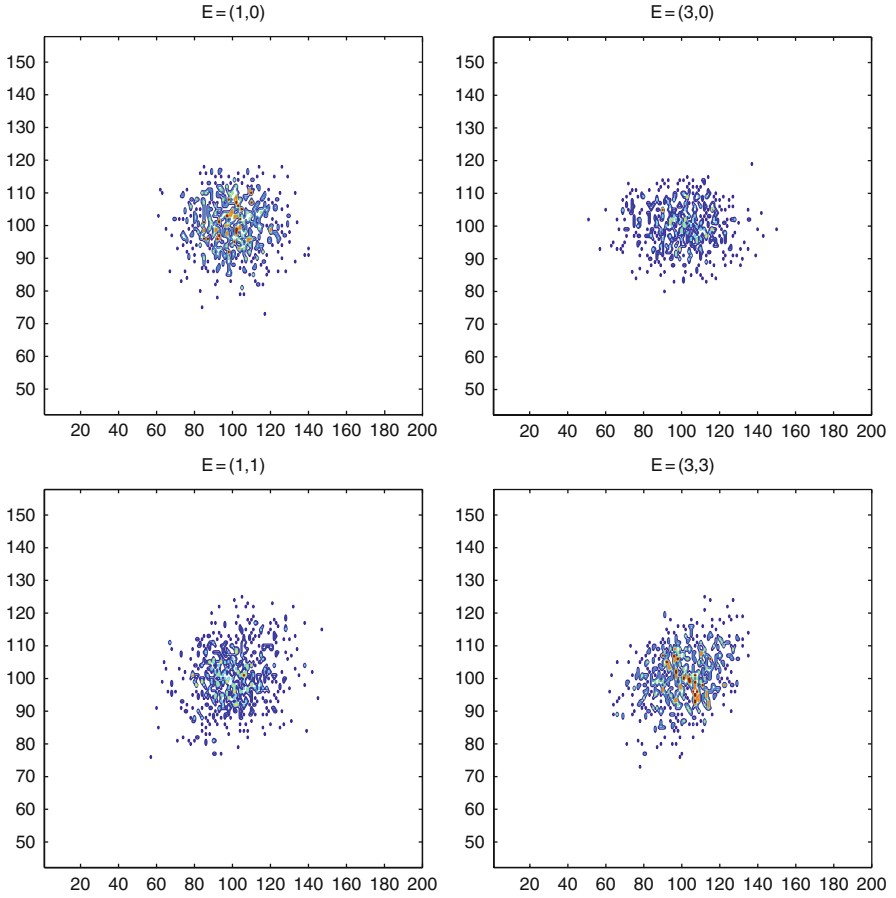


**Fig. 13.13** Time evolution of the pattern for four different tensor fields (after 100 time steps). We observe the elongation of the ellipsoidal cell cluster when the field strength is increased. Above each figure the principal eigenvector of the tensor field is denoted. The initial conditions consist always of a small cluster of cells in the center of the lattice. Different grey levels indicate different cell densities (as in Fig. 13.10)

of brain tumor growth and show the effect of fiber tracts on tumor growth using the DTI information.

## 13.6 Analysis of the LGCA Models for Motion in Static Environments

In this section, we provide a theoretical analysis of the proposed LGCA models. Our aim is to calculate the equilibrium cell distribution and to estimate the speed of cell dispersion under different environments. Finally, we compare our theoretical results with the computer simulations.

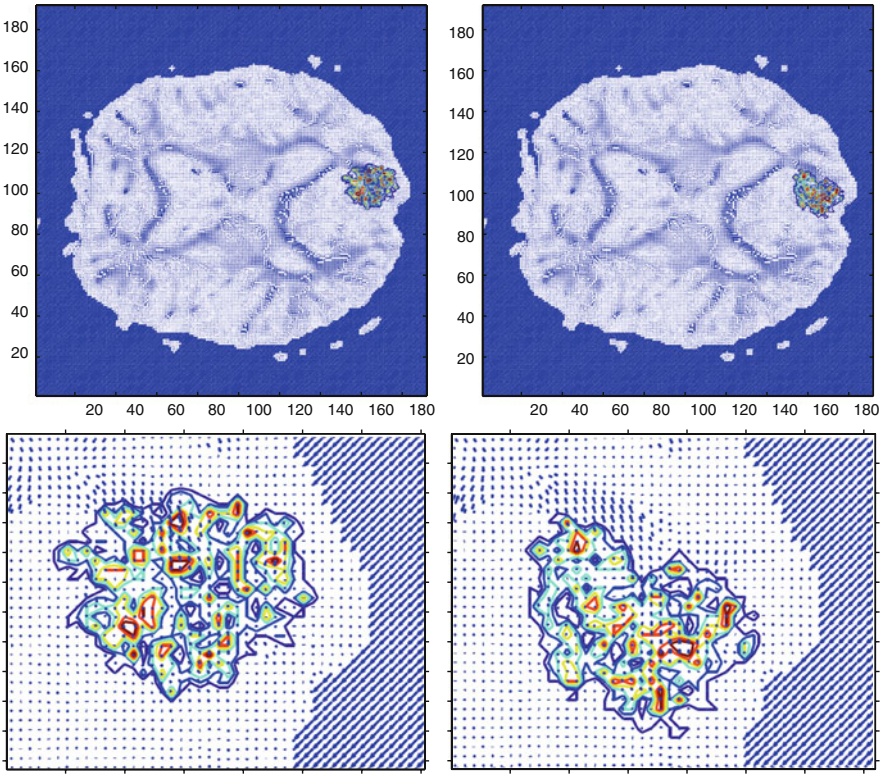


**Fig. 13.14** The effect of the brain's fiber tracts on brain tumor growth: We use a LGCA model of a proliferating (glioma) cancer cell population (for definition see [21]) moving in a tensor field provided by clinical DTI (Diffusion Tensor Imaging) data, representing the brain's fiber tracts. *Top*: the *left figure* shows a simulation without any environmental bias of the cell motion (i.e. cells perform random walks). In the *top right* figure, DTI information is incorporated; the simulation exhibits the anisotropy of a brain tumor due to the effect of the fiber tracts. *Bottom*: Magnifications of the tumor region in the simulations above. Simulations indicate how environmental heterogeneities can affect cell migration and invasion

### *13.6.1 Model I*

In this subsection, we analyze model I and we derive an estimate of the cell spreading speed in dependence of the environmental field strength. The first idea is to choose a macroscopically accessible observable that can be measured experimentally. A reasonable choice is the mean lattice flux $\langle \mathbf{J}(\eta^{\mathrm{C}})\rangle_{\mathbf{E}}$, which characterizes the mean motion of the cells, with respect to changes of the field's strength $|\mathbf{E}|$:

$$\langle \mathbf{J}(\eta^{\mathrm{C}})\rangle_{\mathbf{E}} = \sum_i \mathbf{c}_i f_i^{\mathrm{eq}}, \tag{13.33}$$

where $f_i^{\mathrm{eq}}$, $i = 1, ..., b$ is the equilibrium density distribution of each channel which, in this case, depends on $\mathbf{E}$. Mathematically, this is the mean flux *response* to changes of the external vector field $\mathbf{E}$. The quantity that measures the linear response of the system to the environmental stimuli is called *susceptibility*:

$$\chi = \frac{\partial \langle \mathbf{J} \rangle_{\mathbf{E}}}{\partial \mathbf{E}}. \tag{13.34}$$

We expand the mean flux in terms of small fields as:

$$\langle \mathbf{J} \rangle_{\mathbf{E}} = \langle \mathbf{J} \rangle_{\mathbf{E}=\mathbf{0}} + \frac{\partial \langle \mathbf{J} \rangle_{\mathbf{E}}}{\partial \mathbf{E}} \mathbf{E} + O(\mathbf{E}^2). \tag{13.35}$$

For the zero-field case, the mean flux is zero since the cells are moving randomly within the medium (diffusion). Accordingly, for small fields $\mathbf{E} = \begin{pmatrix} e_1 \\ e_2 \end{pmatrix}$ the linear approximation reads

$$\langle \mathbf{J} \rangle_{\mathbf{E}} = \frac{\partial \langle \mathbf{J} \rangle_{\mathbf{E}}}{\partial \mathbf{E}} \mathbf{E}.$$

The *general linear response relation* is

$$\langle \mathbf{J}(\eta^{\mathrm{C}}) \rangle_{\mathbf{E}} = \chi_{\alpha\beta} e_\beta = \chi e_\alpha, \tag{13.36}$$

where the second rank tensor $\chi_{\alpha\beta}$ is assumed to be isotropic, i.e. $\chi_{\alpha\beta} = \chi \delta_{\alpha\beta}$. Note that we have used Einstein's notation for the sums (summation is implied for repetitive indices) and tensors.

The aim is to estimate the stationary mean flux for fields $\mathbf{E}$. At first, we have to calculate the equilibrium distribution that depends on the external field. The external drive destroys the detailed balance (DB) conditions[2] that would lead to a Gibbs equilibrium distribution. In the case of non-zero external field, the system is out of equilibrium. The external field (environment) induces a breakdown of the spatial symmetry which leads to non-trivial equilibrium distributions depending on the details of the transition probabilities. The (Fermi) exclusion principle allows us to assume that the equilibrium distribution follows a kind of Fermi-Dirac distribution [20]:

[2] The detailed balance (DB) and the semi-detailed balance (SDB) impose the following condition for the microscopic transition probabilities: $\mathbb{P}(\eta \to \eta^{\mathrm{C}}) = \mathbb{P}(\eta^{\mathrm{C}} \to \eta)$ and $\forall \eta^{\mathrm{C}} \in \mathcal{E} : \sum_\eta \mathbb{P}(\eta \to \eta^{\mathrm{C}}) = 1$. Intuitively, the DB condition means that the system jumps to a new micro-configuration and comes back to the old one with the same probability (micro-reversibility). The relaxed SDB does not imply this symmetry. However, the SDB guarantees the existence of steady states and the sole dependence of the Gibbs steady state distribution on the invariants of the system (conserved quantities).

$$f_i^{\mathrm{eq}} = \frac{1}{1 + e^{x(\mathbf{E})}}, \tag{13.37}$$

where $x(\mathbf{E})$ is a quantity that depends on the field $\mathbf{E}$ and the mass of the system (if the DB conditions were fulfilled, the argument of the exponential would depend only on the invariants of the system). Moreover, the sigmoidal form of Eq. (13.37) ensures the positivity of the probabilities $f_i^{\mathrm{eq}} \geq 0$, $\forall x(\mathbf{E}) \in \mathbb{R}$. Thus, one can write the following *ansatz*:

$$x(\mathbf{E}) = h_0 + h_1 \mathbf{c}_i \mathbf{E} + h_2 \mathbf{E}^2. \tag{13.38}$$

After some algebra (the details can be found in [22]), for small fields $\mathbf{E}$, one finds that the equilibrium distribution looks like:

$$f_i^{\mathrm{eq}} = d + d(d-1)h_1 \mathbf{c}_i \mathbf{E} + \frac{1}{2} d(d-1)(2d-1)h_1^2 \sum_{\alpha} c_{i\alpha}^2 e_\alpha^2 + d(d-1)h_2 \mathbf{E}^2, \tag{13.39}$$

where $d = \rho/b$ and $\rho = \sum_{i=1}^{b} f_i^{\mathrm{eq}}$ is the mean node density (which coincides with the macroscopic cell density) and the parameters $h_1, h_2$ have to be determined. Using the mass conservation condition, we find a relation between the two parameters:

$$h_2 = \frac{1 - 2d}{4} h_1^2. \tag{13.40}$$

Finally, the equilibrium distribution can be explicitly calculated for small driving fields:

$$f_i^{\mathrm{eq}} = d + d(d-1)h_1 \mathbf{c}_i \mathbf{E} + \frac{1}{2} d(d-1)(2d-1)h_1^2 Q_{\alpha\beta} e_\alpha e_\beta, \tag{13.41}$$

where $Q_{\alpha\beta} = c_{i\alpha} c_{i\beta} - \frac{1}{2}\delta_{\alpha\beta}$ is a second order tensor.

If we calculate the mean flux, using the equilibrium distribution up to first order terms of $\mathbf{E}$, we obtain from Eq. (13.33) the linear response relation:

$$\langle \mathbf{J}(\eta^C) \rangle = \sum_i c_{i\alpha} f_i^{\mathrm{eq}} = \frac{b}{2} d(d-1) h_1 \mathbf{E}. \tag{13.42}$$

Thus, the susceptibility reads:

$$\chi = \frac{1}{2} bd(d-1)h_1 = -\frac{1}{2} b g_{\mathrm{eq}} h_1, \tag{13.43}$$

where $g_{\mathrm{eq}} = f_i^{\mathrm{eq}}(1 - f_i^{\mathrm{eq}})$ is the equilibrium single particle fluctuation. In [11], the equilibrium distribution is directly calculated from the non-linear lattice Boltzmann equation corresponding to a LGCA with the same rule for small external fields. In

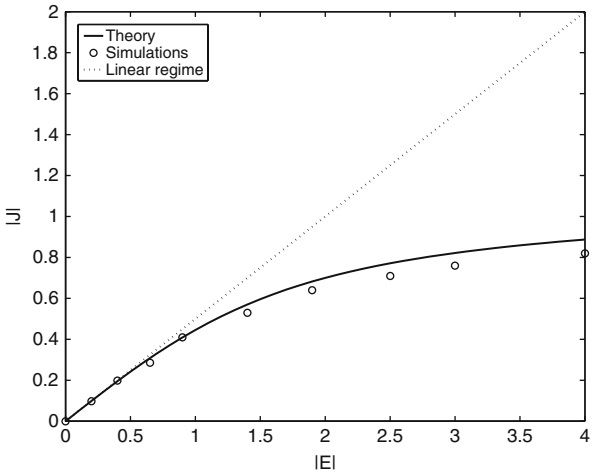


**Fig. 13.15** This figure shows the variation of the normalized measure of the total lattice flux $|\mathbf{J}|$ against the field intensity $|\mathbf{E}|$, where $\mathbf{E} = (e_1, e_2)$. We compare the simulated values with the theoretical calculations (for the linear and non-linear theory). We observe that the linear theory predicts the flux strength for low field intensities. Using the full distribution, the theoretical flux is close to the simulated values also for larger field strengths

the same work, the corresponding susceptibility is determined and this result coincides with ours for $h_1 = -1$. Accordingly, we consider $h_1 = -1$ in the following.

Our method allows us to proceed beyond the linear case, since we have explicitly calculated the equilibrium distribution of our LGCA:

$$f_i^{\mathrm{eq}} = \frac{1}{1 + \exp\left(ln(\frac{1-d}{d}) - \mathbf{c}_i\mathbf{E} + \frac{1-2d}{4}\mathbf{E}^2\right)}. \tag{13.44}$$

Using the definition of the mean lattice flux Eq. (13.33), we can obtain a good theoretical estimation for larger values of the field. Figure 13.15 shows the behavior of the system's normalized flux obtained by simulations and a comparison with our theoretical findings. For small values of the field intensity $|\mathbf{E}|$ the linear approximation performs rather well and for larger values the agreement of our non-linear estimate with the simulated values is more than satisfactory. One observes that the flux response to large fields saturates. This is a biologically plausible result, since the cell speed is finite and an infinite increase of the field intensity cannot lead to infinite fluxes (the mean flux is proportional to the mean velocity). Experimental findings in systems of cell migration mediated by adhesion receptors, such as ECM integrins, support the model's behavior [27, 34].

### *13.6.2 Model II*

In the following section, our analysis characterizes cell motion by a different measurable macroscopic variable and provides an estimate of the cell dispersion for

model II. In this case, it is obvious that the average flux, defined in Eq. (13.33), is zero (due to the symmetry of the interaction rule). In order to measure the anisotropy, we introduce the flux difference between $\mathbf{v}_1$ and $\mathbf{v}_2$, where the $\mathbf{v}_i$'s are eigenvectors of the anisotropy matrix (they are linear combinations of the $\mathbf{c}_i$'s). For simplicity of the calculations, we consider $b = 4$ and X-Y anisotropy. We define:

$$|\langle \mathbf{J}_{\mathbf{v}_1} \rangle - \langle \mathbf{J}_{\mathbf{v}_2} \rangle| = |\langle \mathbf{J}_{x^+} \rangle - \langle \mathbf{J}_{y^+} \rangle| = |c_{11} f_1^{\mathrm{eq}} - c_{22} f_2^{\mathrm{eq}}|. \tag{13.45}$$

As before, we expand the equilibrium distribution around the field $\mathbf{E} = \mathbf{0}$ and we obtain equation

$$f_i = f_i(\mathbf{E} = \mathbf{0}) + (\nabla_{\mathbf{E}}) f_i \mathbf{E} + \frac{1}{2} \mathbf{E}^T (\nabla^2_{\mathbf{E}}) f_i \mathbf{E}. \tag{13.46}$$

With similar arguments as for the previous model I, we can assume that the equilibrium distribution follows a kind of Fermi-Dirac distribution (compare with Eq. (13.37)). This time our *ansatz* has the following form,

$$x(\mathbf{E}) = h_0 + h_1 |\mathbf{c}_i \mathbf{E}| + h_2 \mathbf{E}^2, \tag{13.47}$$

because the rule is symmetric under the inversion $\mathbf{c}_i \rightarrow -\mathbf{c}_i$. Conducting similar calculations as in the previous subsection, one can derive the following expression for the equilibrium distribution:

$$\begin{aligned} f_i^{\mathrm{eq}} = {} & d + d(d-1) h_1 |\mathbf{c}_i \mathbf{E}| \\ & + \frac{1}{2} d(d-1)(2d-1) h_1^2 \sum_\alpha c_{i\alpha}^2 e_\alpha^2 \\ & + d(d-1)(2d-1) h_1^2 |c_{i\alpha} c_{i\beta}| e_\alpha e_\beta \\ & + d(d-1) h_2 \mathbf{E}^2. \end{aligned} \tag{13.48}$$

Here, we identify a relation between $h_1$ and $h_2$ using the microscopic mass conservation law. To simplify the calculations we assume a square lattice (similar calculations can also be carried out for the hexagonal lattice case) and using $c_{11} = c_{22} = 1$, we derive the difference of fluxes along the X-Y axes (we restrict ourselves here to the linear approximation):

$$|f_1^{\mathrm{eq}} - f_2^{\mathrm{eq}}| = d(d-1) h_1 \left| \sum_\alpha |c_{1\alpha}| e_\alpha - \sum_\alpha |c_{2\alpha}| e_\alpha \right| = d(d-1) h_1 |e_1 - e_2|. \tag{13.49}$$

We observe that the parameter $h_1$ is still free and we should find a way to calculate it. Using a method similar to the work of [11] and we find that $h_1 = -1/2$. Substituting this value into the last relation and comparing with simulations (Fig. 13.16), we observe again a very good agreement between the linear approximation and the simulations.

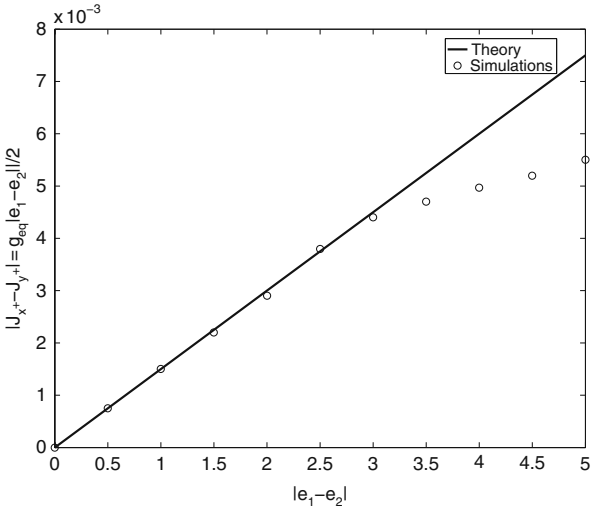


**Fig. 13.16** The figure shows the variation of the X-Y flux difference against the anisotropy strength (according to Model II). We compare the simulated values with the linear theory and observe a good agreement for low anisotropy strength ($|e_1 - e_2| \leq 3$). We observe that the range of agreement, in the linear theory, is larger than in the case of model I

## 13.7 Discussion

In this chapter, we focus on the collective behavior emerging in interacting cell populations. The analysis of collective behavior of interacting cell systems is important for the understanding of phenomena such as morphogenesis, wound healing, tissue growth, tumor invasion etc. We are interested in finding appropriate mathematical models that allow for the description and the analysis of populations composed of discrete, interacting cells. Cellular automata, and particularly LGCA, provide a discrete modeling approach, where a micro-scale investigation is allowed through a stochastic description of the dynamics at the cellular level [15]. In this chapter, we have provided two examples of LGCA models: (i) the collective dynamics of a growing cell population and (ii) the macroscopic behavior of a cell population interacting with its microenvironment.

The first example addresses the collective behavior of a proliferating cell population. Simulations show that growing populations trigger a traveling invasion front, i.e. the growing cell population can be viewed as a wavefront that propagates into its surrounding environment. Via the cut-off mean-field analysis of the discrete LBE, we derive a reaction-diffusion equation that describes our system macroscopically. This cut-off reaction-diffusion equation enables us to calculate accurately the speed of the wavefront. We predict the front velocity to scale with the square root of the product of rates for mitosis and migration. This means that we are able to derive the expansion speed of growing cell populations by incorporating experimentally accessible parameters, as the mitotic and cell motility rates, respectively.

To study and analyze the effects of the microenvironment on cell migration, we have introduced a further LGCA model. We have identified and modeled the two main effects of static environments on cell migration:

- Model I addresses motion in an environment providing directional information. Such environments can be mediated by integrin (adhesive ECM molecules) density gradient fields or diffusible chemical signals leading to haptotactical or chemotactical movement, respectively. We have carried out simulations for different static fields, in order to understand the environmental effect on pattern formation. The main conclusion is that such an environment favors the collective motion of the cells in the direction of the gradients. Interestingly, we observe in Fig. 13.10 that the cell population approximately keeps the shape of the initial cluster and moves in the same direction. This suggests that collective motion is not necessary an alternative cell migration strategy, as described in [19]. Collective motion can be interpreted as emergent behavior in a population of amoeboidly moving cells in a directed environment. Finally, we have calculated theoretically an estimator of the cell spreading speed, i.e. the mean flux for variations of the gradient field strength. The results exhibit a positive response of the cell flux to an increasing field strength. The saturation of the response for large stimuli emphasizes the biological relevance of the model.
- Model II describes cell migration in an environment that influences the orientation of the cells (e.g. alignment). Fibrillar ECMs induce cell alignment and can be considered as an example of an environment that affects cell orientation. Simulations show that such motion produces alignment along a principal orientation (i.e. fiber) and the cells tend to disperse along it (Fig. 13.12). We have calculated the cell response to variations of the field strength, in terms of the flux difference between the principal axis of motion and its perpendicular axis. This difference gives us an estimate of the speed and the direction of cell dispersion. Finally, we observe a similar saturation plateau for large fields, as in model I. Moreover, we gave an application of the second model for the case of brain tumor growth using DTI data (Fig. 13.14).
- The microenvironment plays also a crucial role in the evolutionary dynamics (as a kind of selective pressure) of evolving cellular systems, in particular cancer [2–4].

In the above examples we have seen that LGCA provide an appropriate modeling framework for the analysis of emergent behavior since they allow for:

- The LGCA rules can mimic the microscopic processes at the cellular level (coarse-grained sub-cellular dynamics). Here we focused on the analysis of two selected microscopic interaction rules. Moreover, we showed that with the help of methods motivated by statistical mechanics, we can estimate the macroscopic behavior of the whole population (e.g. mean flux).
- Cell motion through heterogeneous media involves phenomena at various spatial and temporal scales. These cannot be captured in a purely macroscopic modeling approach. In macroscopic models of heterogeneous media diffusion is treated by

using powerful methods that homogenize the environment by the definition of an effective diffusion coefficient (the homogenization process can be perceived as an intelligent averaging of the environment in terms of diffusion coefficients). Continuous limits and effective descriptions require characteristic scales to be bounded and their validity lies far above these bounds [23]. In particular, it is found that in motion through heterogeneous media, anomalous diffusion (subdiffusion) describes the particles' movement over relevant experimental time scales, particularly if the environment is fractal [29]; existing macroscopic continuum equations can not describe such phenomena. On the other hand, discrete microscopic models, like LGCA, can capture different spatio-temporal scales and they are well-suited for simulating such phenomena.

- Moreover, the discrete structure of the LGCA facilitates the implementation of complicated environments (in the form of tensor fields) without any of the computational problems characterizing continuous models.
- LGCA are examples of parallel algorithms. This fact makes them computationally very efficient.

The mean-field (Boltzmann) equation characterizing a given LGCA model arises under the assumption that the probability of finding two cells at specific positions is given by the product of corresponding single particle distribution functions, i.e. any correlations are neglected and distributions fully factorize. It is a challenge to include two-, three-, etc. particle distribution functions which will allow a systematic study of correlation effects. This analysis could particularly improve our understanding of short and long time behavior. In particular, in the case of a traveling front expansion (see above) we have indicated the importance of such correlations at the tip of the front.

The need for discrete models, especially cellular automata, goes beyond the analysis of collective behavior in interacting cell populations. A discrete cell-oriented approach is also required if the dynamic system behavior depends on fluctuations at the individual cell level. This is, for example, the case at the front of invading tumors and crucial for the formation of metastases. Lately, experimental findings of Bru et al. [8] indicate that many tumors share the same surface dynamics. This finding motivated the analysis of the tumor interface by means of a fractal scaling analysis. Obviously, corresponding cancer models have also to be of a discrete nature and CA models are promising candidates to identify growth mechanisms that lead to a particular scaling.

Based on the variability in the local dynamics, an "interaction-module oriented" cellular automaton modeling provides an intuitive and powerful approach to capture essential aspects of complex phenomena at various scales [15]. In conclusion, there are both challenging future perspectives with regards to interesting biological applications of the lattice-gas cellular automaton idea and possible refinements of analytical tools for the investigation of lattice-gas cellular automata. The potential of cellular automata for modeling essential aspects of biological systems will be further exploited in the future.

## References


1. F.J. Alexander, I.Edrei, P.L. Garrido, J.L. Lebowitz, Phase transitions in a probabilistic cellular automaton: growth kinetics and critical properties. J. Statist. Phys. **68**(3/4), 497–514, (1992)
2. A.R. Anderson, A.M. Weaver, P.T. Cummings, V. Quaranta, Tumor morphology and phenotypic evolution driven by selective pressure from the microenvironment. Cell **127**(5), 905–915, (2006)
3. D. Basanta, H. Hatzikirou, A. Deutsch, The emergence of invasiveness in tumours: A game theoretic approach. Eur. Phys. J. B **63**, 393–397, (2008)
4. D. Basanta, M. Simon, H. Hatzikirou, A. Deutsch, An evolutionary game theory perspective elucidates the role of glycolysis in tumour invasion. Cell Prolif. **41**, 980–987, (2008)
5. R.D. Benguria, M.C. Depassier, V. Mendez, Propagation of fronts of a reaction-convection-diffusion equation. Phys. Rev. E **69**, 031106, (2004)
6. D. Bray, *Cell Movements* (Garland Publishing, New York, 1992)
7. H.P. Breuer, W. Huber, F. Petruccione, Fluctuation effects on wave propagation in a reaction-diffusion process. Phys. D **73**, 259, (1994)
8. A. Bru, S. Albertos, J.L. Subiza, J. Lopez Garcia-Asenjo, I. Bru, The universal dynamics of tumor growth. Bioph. J. **85**, 2948–2961, (2003)
9. I. Brunet, B. Derrida Shift in the velocity of a front due to a cutoff. Phys. Rev. E **56**(3), 2597–2604, (1997)
10. I. Brunet, B. Derrida Effect of microscopic noise in front propagation. J. Stat. Phys. **103**(1/2), 269–282, (2001)
11. H. Bussemaker, Analysis of a pattern forming lattice gas automaton: Mean field theory and beyond. Phys. Rev. E **53**(4), 1644–1661, (1996)
12. S.B. Carter, Principles of cell motility: the direction of cell movement and cancer invasion. Nature **208**(5016), 1183–1187, (1965)
13. B. Chopard, M. Droz, *Cellular Automata Modeling of Physical Systems* (Cambridge University Press, Cambridge, 1998)
14. E. Cohen, D. Kessler, H. Levine, Fluctuation-regularized front propagation dynamics in reaction-diffusion systems. Phys. Rev. Lett. **94**, 158302, (2005)
15. A. Deutsch, S. Dormann, *Cellular Automaton Modeling of Biological Pattern Formation* (Birkhäuser, Basel 2005)
16. R.B. Dickinson, R.T. Tranquillo, A stochastic model for cell random motility and haptotaxis based on adhesion receptor fuctuations. J. Math. Biol. **31**, 563–600, (1993).
17. G.D. Doolen, *Lattice Gas Methods for Partial Differential Equations* (Addison-Wesley, New York, 1990)
18. D. Drasdo, S. Höhme, Individual-based approaches to birth and death in avascular tumors. Math. Comp. Model. **37**, 1163–1175, (2003)
19. P. Friedl, Prespecification and plasticity: shifting mechanisms of cell migration. Curr. Opin. Cell. Biol. **16**(1), 14–23, (2004)
20. U. Frisch, D. d'Humieres, B. Hasslacher, P. Lallemand, Y. Pomeau, J.P. Rivet, Lattice gas hydrodynamics in two and three dimensions. Compl. Syst. **1**, 649–707, (1987)
21. H. Hatzikirou, L. Brusch, C. Schaller, M. Simon, A. Deutsch, Prediction of traveling front behavior in a lattice-gas cellular automaton model for tumor invasion. Comput. Math. Appl. **59**, 2326–2339, (2010)
22. H. Hatzikirou, A. Deutsch, Cellular automata as microscopic models of cell migration in heterogeneous environments. Curr. Top. Dev. Biol. **81**, 401–434, (2008)
23. A. Lesne, Discrete vs continuous controversy in physics. Math. Struct. Comp. Sc. **17**(2), 185–223, (2007)
24. J.B. McCarthy, L.T. Furcht, Laminin and fibronectin promote the haptotactic migration of b16 mouse melanoma cells. J. Cell Biol. **98**(4), 1474–1480, (1984)
25. H. Meinhardt, *Models of Biological Pattern Formation* (Academic New York, 1982)
26. J. Murray, *Mathematical Biology I: An Introduction* (Springer, Heidelberg 2001)

27. S.P. Palecek, J.C. Loftus, M.H. Ginsberg, D.A. Lauffenburger, A. F. Horwitz, Integrin-ligand binding governs cell-substratum adhesiveness. Nature **388**(6638), 210, (1997)
28. D.H. Rothman, S. Zaleski, Lattice-gas models of phase separation: interfaces, phase transitions, and multiphase flow. Rev. Mod. Phys. **66**(4), 1417–1479, (1994)
29. M. Saxton, Anomalous diffusion due to obstacles: a Monte Carlo study. Biophys. J. **66**, 394–401, (1994)
30. M.V. Velikanov, R. Kapral, Fluctuation effects on quadratic autocatalysis fronts. J. Chem. Phys. **110**, 109–115, (1999)
31. J. von Neumann, *Theory of Self-Reproducing Automata* (University of Illinois Press, Urbana, IL, 1966)
32. D.A. Wolf-Gladrow, *Lattice-gas Cellular Automata and Lattice Boltzmann Models: An Introduction* (Springer, Heidelberg 2005)
33. S. Wolfram, *A New Kind of Science* (Wolfram Media, Inc., Champaign, IL 2002)
34. M.H. Zaman, P. Matsudaira, D.A. Lauffenburger, Understanding effects of matrix protease and matrix organization on directional persistence and translational speed in three-dimensional cell migration. Ann. Biomed. Eng. **35**(1), 91–100, (2006)